HHS Public Access

Author manuscript

Mol Cancer Ther. Author manuscript; available in PMC 2016 December 01.

Published in final edited form as:

Mol Cancer Ther. 2015 December ; 14(12): 2901–2908. doi:10.1158/1535-7163.MCT-15-0217.

Acute tumor lactate perturbations as a biomarker of genotoxic stress: development of a biochemical model

Vlad C. Sandulache[1,2,*], **Yunyun Chen**[2,*], **Heath D. Skinner**[3], **Tongtong Lu**[2,#], **Lei Feng**[8], **Laurence E. Court**[5], **Jeffrey N. Myers**[2], **Raymond E. Meyn**[4], **Clifton D. Fuller**[3], **James A. Bankson**[6], and **Stephen Y. Lai**[2,7]

[1]Bobby R. Alford Department of Otolaryngology - Head and Neck Surgery, Baylor College of Medicine, Houston, Texas

[2]Department of Head and Neck Surgery, The University of Texas MD Anderson Cancer Center, Houston, Texas

[3]Department of Radiation Oncology, The University of Texas MD Anderson Cancer Center, Houston, Texas

[4]Department of Experimental Radiation Oncology, The University of Texas MD Anderson Cancer Center, Houston, Texas

[5]Department of Imaging Physics, The University of Texas MD Anderson Cancer Center, Houston, Texas

[6]Department of Radiation Physics, The University of Texas MD Anderson Cancer Center, Houston, TX

[7]Department of Molecular and Cellular Oncology, The University of Texas MD Anderson Cancer Center, Houston, Texas

[8]Department of Biostatistics, The University of Texas MD Anderson Cancer Center, Houston, Texas

Abstract

Ionizing radiation is the primary non-surgical treatment modality for solid tumors. Its effectiveness is impacted by temporal constraints such as fractionation, hypoxia and development of radioresistant clones. Biomarkers of acute radiation response are essential to developing more effective clinical algorithms. We hypothesized that acute perturbations in tumor lactate levels act as a surrogate marker of radiation response. *In vitro* experiments were carried out using validated human derived cell lines from 3 histologies: anaplastic thyroid carcinoma (ATC), head and neck squamous cell carcinoma (HNSCC) and papillary thyroid carcinoma (PTC). Cellular metabolic

Corresponding author: Stephen Y. Lai MD, PhD, The University of Texas MD Anderson Cancer Center, 1515 Holcombe Blvd, Unit 1445, Houston, TX 77030, Room Number: FCT10.6002, Phone: (713) 792-6528, Fax: (713) 794-4662, sylai@mdanderson.org.

*Both authors contributed equally to this work.

#Current address: Department of Oral and Maxillofacial Surgery, No. 1 Hospital of Qinhuangdao City, Hebei Province, China

C.D. Fuller reports receiving a commercial research grant from General Electric and Elekta AB and reports receiving speakers bureau honoraria from University of Texas MD Anderson Gilbert Fletcher Society and is a consultant/advisory board member for Elekta AB. The other authors disclose no potential conflicts of interest

activity was measured using standard biochemical assays. *In vivo* validation was performed using both an orthotopic and a flank derivative of a previously established ATC xenograft murine model. Irradiation of cells and tumors triggered a rapid, dose-dependent, transient decrease in lactate levels which was reversed by free radical scavengers. Acute lactate perturbations following irradiation could identify hypoxic conditions and correlated with hypoxia-induced radioresistance. Mutant TP53 cells and cells in which p53 activity was abrogated (shRNA) demonstrated a blunted lactate response to irradiation, consistent with a radioresistant phenotype. Lactate measurements therefore rapidly detected both induced (i.e. hypoxia) and intrinsic (i.e. mutTP53 driven) radioresistance. We conclude that lactate is a quantitative biomarker of acute genotoxic stress, with a temporal resolution which can inform clinical decision-making. Combined with the spatial resolution of newly developed metabolic imaging platforms, this biomarker could lead to the development of truly individualized treatment strategies.

Introduction

Ionizing radiation (IR) is the most effective spatially distributed non-surgical cancer treatment.(1, 2) Through continued technological improvements in IR delivery, definitive treatment doses can now be delivered with decreased toxicity and improved efficacy.(3) Continued improvement in the therapeutic index of IR requires approaches with sufficient temporal resolution to address optimal fractionation, adaptation to transient hypoxia and synergistic incorporation of radiosensitizing agents.(4)

It has been shown, by our group and others, that IR cytotoxicity is largely mediated through generation of reactive oxygen species (ROS) resulting in DNA damage.(5–10) IR-induced ROS perturb cellular metabolism in a measurable and quantifiable manner which could theoretically be exploited for therapeutic purposes.(5) Our group has demonstrated a proportional relationship between IR-induced ROS levels and cell death, and showed that this relationship at least partially accounts for some of the radioresistance encountered in solid tumors.(6, 8) This relationship identifies an important therapeutic window to target radioresistant tumors, such as those driven by mutations in TP53.(6, 8) Although high levels of ROS are essential to achieving a therapeutic effect, basal ROS play an important role in tumorigenesis and metastasis.(11, 12) Because of this dual role, quantitative measurements of tumor cell and tumor ROS are important to maximize therapeutic efficacy and decrease normal tissue toxicity.

Lactate is a metabolite well known to correlate with changes in tissue ROS levels. This relationship has been shown to be important in both normal aging and oncogenic transformation.(13) Brizel and colleagues showed that increased tumor lactate levels correlate with increased metastasis.(13) Quennet et al. extended this initial work to demonstrate that lactate levels correlate with tumor cell relative radiosensitivity.(14) On the basis of this and other promising pre-clinical data, Le et al. conducted a potentially paradigm changing clinical trial, testing the potential of tumor lactate levels to predict treatment response in head and neck tumors.(15, 16) Unfortunately, data generated by this trial failed to demonstrate a correlation between proton magnetic resonance spectroscopic measurements of lactate signal intensity and clinical outcomes.(16)

These data generated a puzzling contradiction between the biochemical promise of lactate and the inability to successfully achieve clinical translation. It has been long established, in both pre-clinical (17, 18) and clinical series (19, 20) that hypoxia exerts a profound impact on *in vivo* radiation effects (21). Matsumoto et al. demonstrated convincingly that lactate perturbations identify hypoxic conditions, a known correlate with induced radioresistance. (22) Furthermore, these metabolic alterations can be linked to genomic alterations such as TP53.(23) Since radiation effectiveness is also mediated by temporal constraints (e.g. fractionation, transient hypoxia, shifting tumor vascularity) we sought to focus on the high-temporal resolution detection of radiation-induced lactate perturbations. Specifically, as microenvironemental lactate levels have long been held as a harbinger of altered radioresistance (24), we hypothesized that IR-induced ROS perturbations are mirrored by rapid changes in tumor cell lactate levels in a measurable and quantifiable manner. This hypothesis is based on previous studies by our group which found that magnetic resonance spectroscopic imaging (MRSI) of hyperpolarized ^{13}C pyruvate can detect acute changes in tumor lactate levels following metabolic inhibition and/or irradiation.(5) In this study, we sought to determine whether measurements of acute lactate changes provide a consistent and reliable means of detecting genotoxic stress with a temporal resolution suitable for clinical translation. To confirm translational relevance we aimed to demonstrate the following: 1) dose-dependent relationship between acute, transient changes in lactate levels and IR exposure; 2) correlation with acquired (i.e. hypoxia) and/or intrinsic (TP53 mutation) radioresistance; and 3) generalizability across multiple histologies.

Materials and Methods

Cells

Previously described cell lines (anaplastic thyroid carcinoma-ATC, papillary thyroid carcinoma-PTC, head and neck squamous cell carcinoma-HNSCC) were obtained from an established cell line bank in the laboratory of Dr. Jeffrey N. Myers under approved institutional protocols. All cell lines were tested and authenticated using short tandem repeat analysis.(25) Cells were maintained in either RPMI of MEM growth media supplemented with glutamine, pyruvate, penicillin/streptomycin and 10% fetal bovine serum. Parental ATC, PTC and HNSCC cell lines were obtained from the above investigator in the last 3 years and are routinely STR tested in our laboratory. HNSCC cell lines containing TP53 constructs have been previously described by our group and were obtained for the experiments detailed here within the last 4 months.(6, 7)

Chemicals

2-deoxyglucose, cobalt (II) chloride, hydrogen peroxide and N-acetyl cysteine (NAC) were purchased from Sigma-Aldrich (St. Louis, MO).

Metabolic studies

For lactate, NAD+ and NADH measurements cells were harvested at various time points (0, 15, 30, 60 and 120 min) post-irradiation (0, 2 and 5 Gy) and/or drug treatment using appropriate buffers and snap-frozen in liquid nitrogen. Lactate, NAD+ and NADH levels

were analyzed by colorimetric assays using commercially available assays (BioVision, Milpitas, CA), according to the manufacturer's instructions.

Cytotoxicity studies

Drug and IR cytotoxicity were assayed using clonogenic assays. Cells were treated with 1mM 2-deoxyglucose for 24 hours, in normoxic (21% O_2) or hypoxic (1% O_2 achieved using hypoxia chamber or CoCl2 exposure) conditions, then irradiated using a high dose-rate ^{137}Cs unit (Mark I-68A,4.5 Gy/min) to the indicated dose (0–6 Gy). Four hours post-irradiation, fresh media were replaced and cells were incubated for colony formation for 10–14 days, then fixed and stained using a 1% formalin/crystal violet solution. Colonies were counted and surviving fractions were determined based upon the plating efficiency of the non-irradiated control group.

ATC tumors

Male athymic nude mice (8–12 weeks) were purchased from the National Cancer Institute (Bethesda, MD), maintained in a pathogen-free facility and fed irradiated mouse chow and autoclaved, reverse osmosis treated water. The animal facility was approved by the American Association for the Accreditation of Laboratory Animal Care and met all current regulations and standards of the U.S. Department of Agriculture, U.S. Department of Health and Human Services and the National Institutes of Health. All procedures were approved by the Institutional Animal Care and Use Committee of The University of Texas M.D. Anderson Cancer Center. For orthotopic tumors, U-HTH83 luciferase expressing cells (2.5×10^5/mouse) were injected into the right thyroid lobe under direct visualization as previously described.(5) For flank tumors, cells (2×10^6/mouse) were injected into both flanks of each animal. Tumor size was ascertained regularly throughout the experimental period using bioluminescence imaging and manual measurements as previously described. (5, 7) Tumors were allowed to grow for 1 week prior to initiation of imaging experiments. Tumors were irradiated to indicated doses (5 Gy) using either a Co^{60} irradiator and custom lead blocks or an image-guided radiotherapy system (X-Rad 225Cx, Precision X-Ray Inc., North Branford, CT). Both irradiation methods delivered the same targeted radiation dose to the same tumor volume. Tumors were harvested for either biochemical analysis or histologic and immunohistochemical analysis. The number of animals chosen for each in vivo experiment was based on previous experience with this animal model and the expected effect size. Statistical analysis of *in vivo* data was conducted as described below.

Statistical analysis

All *in vitro* experiments were carried out at least in triplicate (for each condition) and were repeated to ensure reproducibility. All statistical analysis for *in vitro* experiments was conducted using two tailed, Student's t-test analysis with a cutoff p-value of 0.05 to demonstrate statistical significance. For all *in vivo* experiments statistical significance was determined using Student's t-test analysis with a cutoff p-value of 0.05 to demonstrate statistical significance.

Results

Oxidative stress perturbs ATC cellular reducing potential

ATC cells were grown under standard conditions and exposed to 2-DG, a known inhibitor of glycolysis and a compound previously shown by us and others to decrease the global cellular reducing potential.(6, 26, 27) This resulted in a significant increase in NAD+ levels (75%) and a drop in the ratio of NADH/NAD+ (50%) consistent with a predicted decrease in reducing potential (Supplemental Figure 1A). These effects were reproduced by exogenous administration of H_2O_2 (Supplemental Figure 1B). N-acetyl cysteine (NAC), a scavenger of reactive oxygen species (ROS) reverses the effects on cellular reducing potential of both 2-DG and H_2O_2 in a concentration-dependent manner (Supplemental Figure 1). Together, these data indicate that the ATC cellular REDOX (reducing equivalent levels) state can be perturbed by metabolic inhibition or exogenous ROS in a measurable, transient and reversible manner.

Ionizing radiation triggers acute perturbations in ATC cellular reducing potential

Ionizing radiation (IR) triggers a rapid, transient increase in cellular ROS which is rapidly scavenged by primary cellular reducing equivalents which are regenerated metabolically (Figure 1A).(12, 28, 29) Exposure of ATC cells to increasing doses of IR resulted in minimal perturbations in total cellular NADH levels (Supplemental Figure 2). In contrast, NAD+ levels increased within minutes of IR exposure and returned to baseline at 2hrs post irradiation (Supplemental Figure 2). This resulted in a transient decrease in the NADH/NAD + cellular ratio which normalized over time (Figure 1B). NAC reversed the effects of IR on the NADH/NAD+ in a concentration-dependent manner, consistent with an ROS-driven mechanism (Figure 1C).

Cellular lactate levels reflect IR-induced alterations in cellular reducing potential

The ultimate step in anaerobic glycolysis reduces pyruvate into lactate using electrons donated by NADH. As such, the conversion rate is an indirect reflection of cellular oxidative stress and the metabolic response to it (Figure 2A). To further demonstrate this biochemical relationship, ATC cells were exposed to metabolic inhibition (2-DG) or oxidative stress (H_2O_2). Lactate production decreased in response to both agents, and effect which was reversed in a concentration-dependent manner by NAC (Figure 2B). Consistent with effects on cellular reducing potential, IR exposure decreased lactate production acutely in a dose-dependent manner; this was reversed by NAC (Figure 2C). This dose-dependent decrease in tumor cell lactate levels correlates with the dose-dependent increase in cell death following irradiation demonstrated using clonogenic survival (Figure 2C). In order to further test the link between ROS and lactate levels following irradiation, H_2O_2 was used to increase tumor cell ROS levels. This resulted in a correspondent increase in the magnitude of tumor cell lactate changes following irradiation, in contrast to the effects of NAC, which restores lactate levels following irradiation (Supplemental Figure 3).

IR exposure acutely decreases ATC tumor lactate levels

For orthotopic tumors, U-HTH83 luciferase expressing cells (2.5×10^5/mouse) were orthotopically injected into the right thyroid lobe under direct visualization as previously described.(5, 30) Tumors were detected by bioluminescence activity using IVIS 200 imaging system (Xenogen Corp., Waltham, MA). For flank ATC xenograft tumors, U-HTH83-*lucif* cells (2×10^6/tumor) were injected subcutaneously into both flanks of each athymic nude mice. The subcutaneous tumors were allowed to grow for 10–12 days before irradiation. Four tumors were maintained as controls and 4 tumors were irradiated using a single fraction of 5 Gy. Tumors were harvested immediately post-irradiation and tumor lactate levels were measured. Lactate levels in tumors exposed to IR were significantly lower than those in control tumors (Figure 3A). The experiment was repeated using orthotopic ATC xenografts which more closely recapitulate human tumor growth and vascularity. As shown in Figure 3B, irradiation (5 Gy) resulted in a significant, acute drop in tumor lactate levels compared to control tumors.

Cellular lactate levels reflect hypoxia-induced radioresistance

Hypoxic conditions can be reproduced using either a hypoxia chamber or chemical inhibition ($CoCl_2$) (Figure 4A). Although most tumor cells, including the ATC cell lines utilized here, are primarily glycolytic at baseline, this metabolic phenotype is exacerbated by either chamber or chemically induced hypoxia as demonstrated by increased baseline lactate generation (Supplemental Figure 4). A similar shift in tumor metabolism is expected under *in vivo* conditions when transient alterations in vascularity induce hypoxic conditions of varying duration. Consistent with an increased glycolytic reliance, ATC cells become more sensitive to the cytotoxic effects of 2-DG under conditions of hypoxia (Figure 4B). Under conditions of hypoxia ($CoCl_2$), the IR-induced transient drop in lactate levels persists, but the magnitude of the effect is reduced by approximately 50% compared to normoxic conditions (Figure 4C). To evaluate the relationship between IR-induced lactate perturbations and IR effects on tumor cell death, we performed clonogenic survival assays in the presence and absence of hypoxia. ATC cells exposed to hypoxia (chamber) exhibited relative radioresistance compared to normoxic conditions at all tested IR doses (Figure 4D). This effect was effectively reversed by the addition of 2-DG.

Cellular lactate levels reflect intrinsic tumor cell radioresistance/radiosensitivity

To test the generalizability of the above described relationship between IR, NADH/NAD+ ratio and lactate levels, were evaluated the response using a pair of previously established human head and neck squamous cell carcinoma (HNSCC) cells lines which are isogenic with the exception for TP53 mutational status.(6, 8) IR triggered a transient, reversible, dose-dependent drop in cellular NADH/NAD+ ratio and lactate levels (Figure 5). Consistent with previously reported relative radioresistance, HN31 (p53 mut) cells demonstrated a blunted decrease in the NADH/NAD+ ratio and cellular lactate levels following irradiation as compared to HN30 (p53 wt) cells. In order to confirm that this differential response is driven by loss of p53 function, we tested the effect of IR on cellular lactate levels using a previously described pair of constructs. As shown in Figure 5, HN30 cells in which p53 activity was decreased by shRNA interference demonstrated a blunted response to IR

compared to lentiviral vector transfected HN30 control cells. At 5 Gy, the drop in lactate levels in shp53 cells was 49% at 15 minutes and 72% at 30 minutes post irradiation. These quantitative differences were reproducible across multiple replicates and experimental series as well as multiple IR doses (Supplemental Figure 5). Specifically, at the lower dose of 2 Gy, the lactate drop in cells with suppressed p53 activity (shp53) was only 36% of that of lentiviral transfected control cells at 15 minutes post-irradiation and 59% at 30 minutes post-irradiation. These data are consistent with our previously published data regarding the relative radioresistance/radiosensitivity of this pair of constructs (Supplemental Figure 6).(6, 8)

We further validated the relationship between cellular lactate levels and acute radiation exposure in a multiple ATC and PTC cell lines. As shown in Figure 6, multiple cell lines demonstrated a consistent drop in lactate levels following irradiation, with return to baseline within several hours post-exposure.

Discussion

Improvements in dose delivery via intensity modulated radiotherapy have resulted in decreased normal tissue toxicity and improved locoregional control through selective boosting of specific tumor regions in the clinical setting.(3) Unfortunately, the lack of high-temporal resolution methods to interrogate the tumor microenvironment precludes selective targeting of tumor subvolumes at increased risk of local recurrence. This means that all volumes of a tumor are currently treated to a uniform volume, despite the fact that subregions of the tumor associated with hypoxia are the regions most likely to recur.(31) Altered fractionation protocols and hypoxia modifiers can greatly impact effectiveness (32–34), yet the optimal regimen remains elusive.(35) While there are several direct imaging markers of hypoxia (36–38), their temporal resolution is relatively poor. Although previously identified genomic, epigenetic and metabolic markers of relative radiosensitivity/radioresistance can provide prognostic information and may guide treatment decisions at a population level, they are less useful for tailoring treatment strategies to individual tumors.(6, 8, 39) What is required is a real-time biomarker of radiation response with sufficient temporal resolution to inform clinical decision making.

In this study, we describe a biochemical model which can transform tumor lactate from an imperfect treatment correlate to an actionable indicator of acute radiation response. Our data indicate that IR-induced ROS decrease tumor cell reducing equivalent levels, resulting in a transient drop in tumor cell lactate levels, consistent with classic historical radiobiological observations, from Tozer et al.(21), indicating lactate reduction postradiotherapy. It is essential to emphasize that this process occurs within minutes following irradiation. This is important for two reasons. First, this time frame is consistent with real-time decision making in the clinical setting. Second, it may at least partially explain previously published negative clinical data.(16) Since lactate levels return to baseline within 2 hours post-irradiation, delayed measurements, or measurements which are widely spaced out during treatment are unlikely to capture the metabolic impact of treatment regimens. The ability to reproduce this effect through exogenous ROS, and reverse it through application of ROS scavengers conclusively links exogenous ROS, tumor reducing potential and lactate levels. The dose

dependence of IR-induced lactate perturbations further demonstrates that this is a quantitative not simply a qualitative relationship.

Utilization of acute lactate perturbations as a real-time biomarker of radiation response can potentially address an additional current clinical constraint: transient hypoxia assessment. Tumor hypoxia demonstrates not only spatial (40) but temporal heterogeneity as well (41), with acute and chronic components(42). Immunohistochemical means of assessing tumor hypoxia are static, and the use of existing metabolic imaging methods are constrained by tumor size-associated spatial heterogeneity (43), variable tracer-specific time dependencies (44), and reported discordance with direct measurement in specific tumor histologies(45). Within a time frame of minutes, lactate levels can be used to distinguish radiation response in hypoxic conditions from its normoxic correlate in a manner consistent with acquired radioresistance. Dynamic integration of this approach via HP-MRSI (5) could allow for daily adaptive fractionation and dose painting designed to overcome hypoxia-induced radioresistance; conceivably, such data could be used to investigate biologically-optimized radiotherapy schedules which might even occur at non-daily intervals or with varying fractionation, as suggested recently by Leder et al.(46)

Intrinsic radioresistance, driven by specific genomic or epigenetic events, has been shown to adversely affect treatment effectiveness.(8, 39, 47) The most common oncogenic event in solid tumors, mutation of the TP53 gene, not only drives tumorigenesis and metastasis, but also contributes to radiation and chemotherapy resistance.(6, 8, 39) Since not all mutations behave identically, and since the remainder of the genomic background can further modulate treatment responsiveness, *a priori* predictions based on TP53 mutational status cannot be used for individual tumor treatment planning. Our data demonstrate that, as in the case of acquired hypoxia, measurements of IR-induced lactate perturbations can distinguish between cells expressing wild-type TP53 and cells expressing mutant TP53 within minutes. It has been well established that solid tumors are heterogeneous with respect to genomic and epigenetic background. This becomes particularly important as clonal populations are obliterated or survive ongoing treatment, and as specific clones begin to repopulate solid tumors during disease recurrence. The ability to temporally resolve shifts in tumor cell populations during disease development and treatment can be a crucial asset to improved clinical effectiveness.

A translationally viable approach to lactate measurements in the clinical setting must be: 1) non-invasive, 2) iterative and 3) capable of resolving biochemical data spatially and temporally. Previous attempts to measure tumor lactate levels using traditional proton magnetic resonance spectroscopy sequences may have been hampered by limited spatial and temporal resolution driven in part by the overlap of lactate (~1.3ppm) and lipid (0.9–1.5ppm) resonance.(16, 48) We have recently published data demonstrating that MRI of hyperpolarized ^{13}C pyruvate (HP-MRI) provides real-time measurements of tumor conversion of pyruvate into lactate with excellent spatial resolution.(5, 7) HP-MRI provides a powerful imaging platform, with greatly improved signal-to-noise ratio compared to traditional proton magnetic resonance spectroscopy.(16, 48, 49) Xu et al. utilized this imaging platform to differentiate between cell lines with high and low metastatic potential.

(15) Thind et al. demonstrated that HP-MRI can be used to detect acute normal tissue radiation toxicity in a lung model.(50)

The biochemical model presented here demonstrates that lactate measurements possess the temporal resolution required for clinical translation. HP-MRI of ^{13}C lactate has demonstrated, in both pre-clinical and clinical trials the spatial resolution required for treatment optimization. Together, these tools provide a unique avenue for development of truly individualized solid tumor treatment strategies.(51) Specifically, we propose two overlapping approaches to improving outcomes following irradiation of solid tumors. First, lactate interrogation can be used in pre-clinical animal models to optimize the timing of radiosensitizing agents such as cisplatin in order to maximize oxidative stress at the moment of tumor irradiation. These data can be tested for increased treatment efficacy in the setting of a clinical trial. Second, lactate interrogation via HP-MRI can be mated to newly available MRI-based irradiation platforms in order to develop adaptive irradiation algorithms which allow for dose adjustment throughout the radiation treatment course in order to maximize therapeutic index.

Supplementary Material

Refer to Web version on PubMed Central for supplementary material.

Acknowledgments

This research was supported in part by Institutional Start-up Funds (S.Y. Lai), the National Cancer Institute (R21 CA178450; S.Y. Lai), the National Institutes of Health Cancer Center Support Grant (P30 CA016672 to J.A. Bankson through R.D. Pinho), and the Cancer Prevention and Research Institute of Texas (RP101243-P5; J.A. Bankson; RP140021-P5; J.A. Bankson). The content is solely the responsibility of the authors and does not necessarily represent the official views of the National Cancer Institute or the National Institutes of Health. The funders had no role in study design, data collection and analysis, decision to publish, or preparation of the manuscript.

References

1. Bhatia A, Rao A, Ang KK, Garden AS, Morrison WH, Rosenthal DI, et al. Anaplastic thyroid cancer: Clinical outcomes with conformal radiotherapy. Head Neck. 2010; 32:829–36. [PubMed: 19885924]
2. Derbel O, Limem S, Segura-Ferlay C, Lifante JC, Carrie C, Peix JL, et al. Results of combined treatment of anaplastic thyroid carcinoma (ATC). BMC Cancer. 2011; 11:469. [PubMed: 22044775]
3. Beadle BM, Liao KP, Elting LS, Buchholz TA, Ang KK, Garden AS, et al. Improved survival using intensity-modulated radiation therapy in head and neck cancers: a SEER-Medicare analysis. Cancer. 2014; 120:702–10. [PubMed: 24421077]
4. Chaplin DJ, Durand RE, Olive PL. Acute hypoxia in tumors: implications for modifiers of radiation effects. Int J Radiat Oncol Biol Phys. 1986; 12:1279–82. [PubMed: 3759546]
5. Sandulache VC, Chen Y, Lee J, Rubinstein A, Ramirez MS, Skinner HD, et al. Evaluation of hyperpolarized [1-(1)(3)C]-pyruvate by magnetic resonance to detect ionizing radiation effects in real time. PLoS One. 2014; 9:e87031. [PubMed: 24475215]
6. Sandulache VC, Skinner HD, Ow TJ, Zhang A, Xia X, Luchak JM, et al. Individualizing antimetabolic treatment strategies for head and neck squamous cell carcinoma based on TP53 mutational status. Cancer. 2012; 118:711–21. [PubMed: 21720999]

7. Sandulache VC, Skinner HD, Wang Y, Chen Y, Dodge CT, Ow TJ, et al. Glycolytic inhibition alters anaplastic thyroid carcinoma tumor metabolism and improves response to conventional chemotherapy and radiation. Mol Cancer Ther. 2012; 11:1373–80. [PubMed: 22572813]
8. Skinner HD, Sandulache VC, Ow TJ, Meyn RE, Yordy JS, Beadle BM, et al. TP53 disruptive mutations lead to head and neck cancer treatment failure through inhibition of radiation-induced senescence. Clin Cancer Res. 2012; 18:290–300. [PubMed: 22090360]
9. Fischer-Nielsen A, Jeding IB, Loft S. Radiation-induced formation of 8-hydroxy-2′-deoxyguanosine and its prevention by scavengers. Carcinogenesis. 1994; 15:1609–12. [PubMed: 8055639]
10. Mohan N, Meltz ML. Induction of nuclear factor kappa B after low-dose ionizing radiation involves a reactive oxygen intermediate signaling pathway. Radiation research. 1994; 140:97–104. [PubMed: 7938461]
11. Kang KA, Kim KC, Bae SC, Hyun JW. Oxidative stress induces proliferation of colorectal cancer cells by inhibiting RUNX3 and activating the Akt signaling pathway. International journal of oncology. 2013; 43:1511–6. [PubMed: 24042352]
12. de Oliveira MF, Amoedo ND, Rumjanek FD. Energy and redox homeostasis in tumor cells. Int J Cell Biol. 2012; 2012:593838. [PubMed: 22693511]
13. Brizel DM, Schroeder T, Scher RL, Walenta S, Clough RW, Dewhirst MW, et al. Elevated tumor lactate concentrations predict for an increased risk of metastases in head-and-neck cancer. Int J Radiat Oncol Biol Phys. 2001; 51:349–53. [PubMed: 11567808]
14. Quennet V, Yaromina A, Zips D, Rosner A, Walenta S, Baumann M, et al. Tumor lactate content predicts for response to fractionated irradiation of human squamous cell carcinomas in nude mice. Radiother Oncol. 2006; 81:130–5. [PubMed: 16973228]
15. Xu HN, Kadlececk S, Profka H, Glickson JD, Rizi R, Li LZ. Is higher lactate an indicator of tumor metastatic risk? A pilot MRS study using hyperpolarized (13)C-pyruvate. Acad Radiol. 2014; 21:223–31. [PubMed: 24439336]
16. Le QT, Koong A, Lieskovsky YY, Narasimhan B, Graves E, Pinto H, et al. In vivo 1H magnetic resonance spectroscopy of lactate in patients with stage IV head and neck squamous cell carcinoma. Int J Radiat Oncol Biol Phys. 2008; 71:1151–7. [PubMed: 18258377]
17. Chaplin DJ, Durand RE, Olive PL. Acute hypoxia in tumors: implications for modifiers of radiation effects. International journal of radiation oncology, biology, physics. 1986; 12:1279–82.
18. Hall EJ. The effect of hypoxia on the repair of sublethal radiation damage in cultured mammalian cells. Radiation research. 1972; 49:405–15. [PubMed: 5058080]
19. Nordsmark M, Bentzen SM, Rudat V, Brizel D, Lartigau E, Stadler P, et al. Prognostic value of tumor oxygenation in 397 head and neck tumors after primary radiation therapy. An international multi-center study. Radiotherapy and oncology: journal of the European Society for Therapeutic Radiology and Oncology. 2005; 77:18–24. [PubMed: 16098619]
20. Brizel DM, Sibley GS, Prosnitz LR, Scher RL, Dewhirst MW. Tumor hypoxia adversely affects the prognosis of carcinoma of the head and neck. International journal of radiation oncology, biology, physics. 1997; 38:285–9.
21. Tozer G, Suit HD, Barlai-Kovach M, Brunengraber H, Biaglow J. Energy metabolism and blood perfusion in a mouse mammary adenocarcinoma during growth and following X irradiation. Radiat Res. 1987; 109:275–93. [PubMed: 3809398]
22. Matsumoto S, Hyodo F, Subramanian S, Devasahayam N, Munasinghe J, Hyodo E, et al. Low-field paramagnetic resonance imaging of tumor oxygenation and glycolytic activity in mice. J Clin Invest. 2008; 118:1965–73. [PubMed: 18431513]
23. Contractor T, Harris CR. p53 negatively regulates transcription of the pyruvate dehydrogenase kinase Pdk2. Cancer research. 2012; 72:560–7. [PubMed: 22123926]
24. Hirschhaeuser F, Sattler UG, Mueller-Klieser W. Lactate: a metabolic key player in cancer. Cancer Research. 2011; 71:6921–5. [PubMed: 22084445]
25. Zhao M, Sano D, Pickering CR, Jasser SA, Henderson YC, Clayman GL, et al. Assembly And Initial Characterization Of A Panel Of 85 Genomically Validated Cell Lines From Diverse Head And Neck Tumor Sites. Clin Cancer Res. 2011; 17:7248–64. [PubMed: 21868764]

26. Sandulache VC, Ow TJ, Pickering CR, Frederick MJ, Zhou G, Fokt I, et al. Glucose, not glutamine, is the dominant energy source required for proliferation and survival of head and neck squamous carcinoma cells. Cancer. 2011; 117:2926–38. [PubMed: 21692052]
27. Simons AL, Ahmad IM, Mattson DM, Dornfeld KJ, Spitz DR. 2-Deoxy-D-glucose combined with cisplatin enhances cytotoxicity via metabolic oxidative stress in human head and neck cancer cells. Cancer research. 2007; 67:3364–70. [PubMed: 17409446]
28. Pollak N, Dolle C, Ziegler M. The power to reduce: pyridine nucleotides--small molecules with a multitude of functions. Biochem J. 2007; 402:205–18. [PubMed: 17295611]
29. Pollycove M, Feinendegen LE. Radiation-induced versus endogenous DNA damage: possible effect of inducible protective responses in mitigating endogenous damage. Hum Exp Toxicol. 2003; 22:290–306. discussion 7, 15–7, 19–23. [PubMed: 12856953]
30. Gule MK, Chen Y, Sano D, Frederick MJ, Zhou G, Zhao M, et al. Targeted therapy of VEGFR2 and EGFR significantly inhibits growth of anaplastic thyroid cancer in an orthotopic murine model. Clin Cancer Res. 2011; 17:2281–91. [PubMed: 21220477]
31. Hoogsteen IJ, Marres HA, Bussink J, van der Kogel AJ, Kaanders JH. Tumor microenvironment in head and neck squamous cell carcinomas: predictive value and clinical relevance of hypoxic markers. A review. Head Neck. 2007; 29:591–604. [PubMed: 17252597]
32. Koukourakis MI. Hypofractionated and accelerated radiotherapy with amifostine cytoprotection (HypoARC): a new concept in radiotherapy and encouraging results in breast cancer. Semin Oncol. 2002; 29:42–6. [PubMed: 12577243]
33. Kaanders JH, Pop LA, Marres HA, Bruaset I, van den Hoogen FJ, Merkx MA, et al. ARCON: experience in 215 patients with advanced head-and-neck cancer. International journal of radiation oncology, biology, physics. 2002; 52:769–78.
34. Bernier J, Denekamp J, Rojas A, Trovo M, Horiot JC, Hamers H, et al. ARCON: accelerated radiotherapy with carbogen and nicotinamide in non small cell lung cancer: a phase I/II study by the EORTC. Radiotherapy and oncology: journal of the European Society for Therapeutic Radiology and Oncology. 1999; 52:149–56. [PubMed: 10577700]
35. Beitler JJ, Zhang Q, Fu KK, Trotti A, Spencer SA, Jones CU, et al. Final results of local-regional control and late toxicity of RTOG 9003: a randomized trial of altered fractionation radiation for locally advanced head and neck cancer. Int J Radiat Oncol Biol Phys. 2014; 89:13–20. [PubMed: 24613816]
36. Matsuo M, Matsumoto S, Mitchell JB, Krishna MC, Camphausen K. Magnetic resonance imaging of the tumor microenvironment in radiotherapy: perfusion, hypoxia, and metabolism. Semin Radiat Oncol. 2014; 24:210–7. [PubMed: 24931096]
37. Servagi-Vernat S, Differding S, Hanin FX, Labar D, Bol A, Lee JA, et al. A prospective clinical study of (1)(8)F-FAZA PET-CT hypoxia imaging in head and neck squamous cell carcinoma before and during radiation therapy. European journal of nuclear medicine and molecular imaging. 2014; 41:1544–52. [PubMed: 24570097]
38. Li L, Yu J, Xing L, Ma K, Zhu H, Guo H, et al. Serial hypoxia imaging with 99mTc-HL91 SPECT to predict radiotherapy response in nonsmall cell lung cancer. Am J Clin Oncol. 2006; 29:628–33. [PubMed: 17149002]
39. Poeta ML, Manola J, Goldwasser MA, Forastiere A, Benoit N, Califano JA, et al. TP53 mutations and survival in squamous-cell carcinoma of the head and neck. N Engl J Med. 2007; 357:2552–61. [PubMed: 18094376]
40. Rofstad EK, Maseide K. Radiobiological and immunohistochemical assessment of hypoxia in human melanoma xenografts: acute and chronic hypoxia in individual tumours. Int J Radiat Biol. 1999; 75:1377–93. [PubMed: 10597912]
41. Kato Y, Yashiro M, Fuyuhiro Y, Kashiwagi S, Matsuoka J, Hirakawa T, et al. Effects of acute and chronic hypoxia on the radiosensitivity of gastric and esophageal cancer cells. Anticancer Res. 2011; 31:3369–75. [PubMed: 21965748]
42. Coleman CN. Hypoxia in tumors: a paradigm for the approach to biochemical and physiologic heterogeneity. J Natl Cancer Inst. 1988; 80:310–7. [PubMed: 3282077]
43. Bentzen L, Keiding S, Horsman MR, Gronroos T, Hansen SB, Overgaard J. Assessment of hypoxia in experimental mice tumours by [18F]fluoromisonidazole PET and pO2 electrode

measurements. Influence of tumour volume and carbogen breathing. Acta Oncol. 2002; 41:304–12. [PubMed: 12195751]

44. Bollineni VR, Koole MJ, Pruim J, Brouwer CL, Wiegman EM, Groen HJ, et al. Dynamics of tumor hypoxia assessed by (18)F-FAZA PET/CT in head and neck and lung cancer patients during chemoradiation: Possible implications for radiotherapy treatment planning strategies. Radiotherapy and oncology: journal of the European Society for Therapeutic Radiology and Oncology. 2014; 113:198–203. [PubMed: 25434768]
45. Bentzen L, Keiding S, Nordsmark M, Falborg L, Hansen SB, Keller J, et al. Tumour oxygenation assessed by 18F-fluoromisonidazole PET and polarographic needle electrodes in human soft tissue tumours. Radiotherapy and oncology: journal of the European Society for Therapeutic Radiology and Oncology. 2003; 67:339–44. [PubMed: 12865184]
46. Leder K, Pitter K, Laplant Q, Hambardzumyan D, Ross BD, Chan TA, et al. Mathematical modeling of PDGF-driven glioblastoma reveals optimized radiation dosing schedules. Cell. 2014; 156:603–16. [PubMed: 24485463]
47. Masica DL, Li S, Douville C, Manola J, Ferris RL, Burtness B, et al. Predicting survival in head and neck squamous cell carcinoma from TP53 mutation. Hum Genet. 2015; 134(5):497–507. [PubMed: 25108461]
48. Kobus T, Wright AJ, Van Asten JJ, Heerschap A, Scheenen TW. In vivo (1) H MR spectroscopic imaging of aggressive prostate cancer: can we detect lactate? Magn Reson Med. 2014; 71:26–34. [PubMed: 23475759]
49. Park I, Chen AP, Zierhut ML, Ozturk-Isik E, Vigneron DB, Nelson SJ. Implementation of 3 T lactate-edited 3D 1H MR spectroscopic imaging with flyback echo-planar readout for gliomas patients. Ann Biomed Eng. 2011; 39:193–204. [PubMed: 20652745]
50. Thind K, Chen A, Friesen-Waldner L, Ouriadov A, Scholl TJ, Fox M, et al. Detection of radiation-induced lung injury using hyperpolarized (13) C magnetic resonance spectroscopy and imaging. Magn Reson Med. 2013; 70:601–609. [PubMed: 23074042]
51. Lai SY, Fuller CD, Bhattacharya PK, Frank SJ. Metabolic Imaging as a Biomarker of Early Radiation Response in Tumors. Clin Cancer Res. 2015 pii: clincanres. 1214.2015. [Epub ahead of print].

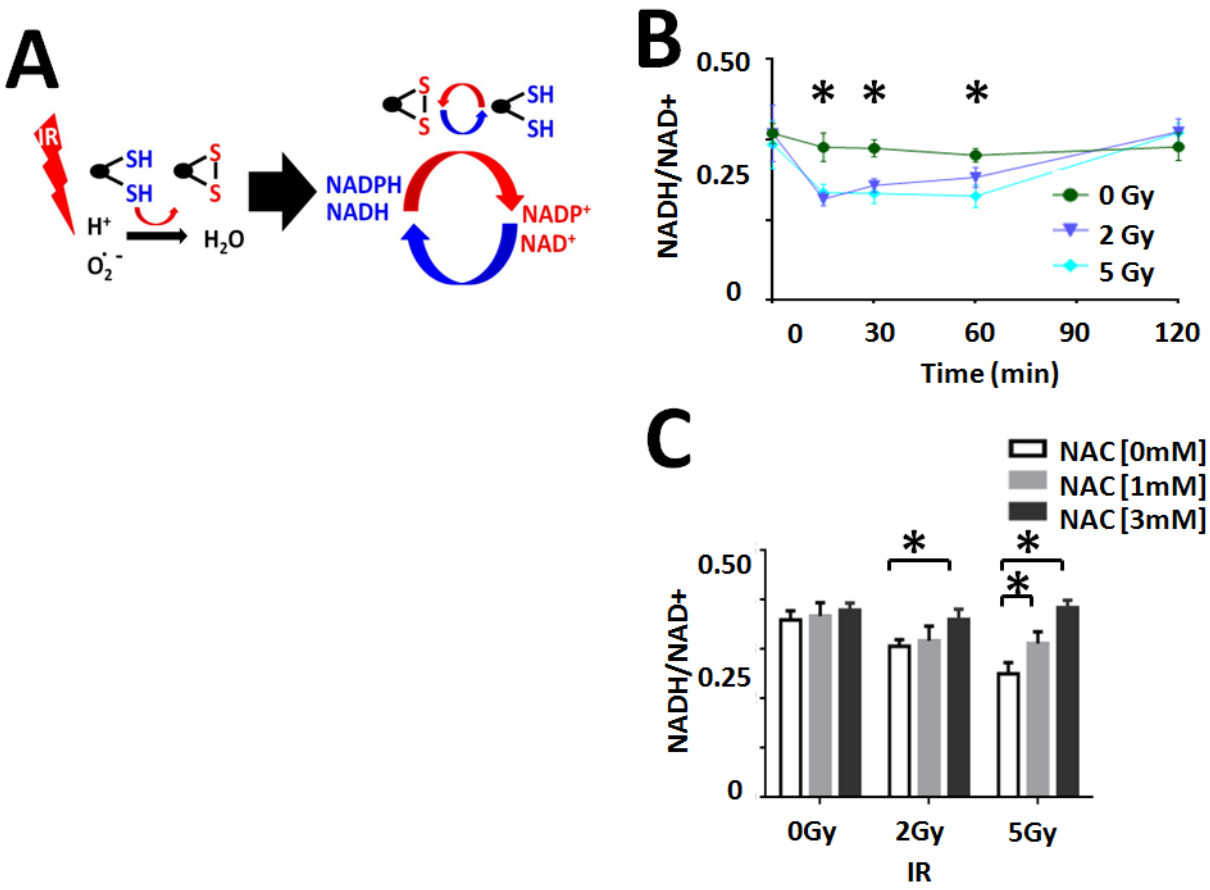

Figure 1. IR triggers a temporary, reversible perturbation in cellular reducing potential

A) Model of hypothesized effects of IR on cellular reducing equivalents. B) Effects on the cellular NADH/NAD+ ratio following exposure to increasing doses of IR. C) Dose-dependent changes in the cellular NADH/NAD+ ratio following exposure to increasing IR doses were reversed by treatment with NAC in a concentration-dependent manner. * indicates p-value < 0.05 compared to corresponding control condition. All values normalized to corresponding control condition (1.0). Each experiment was carried out at least in triplicate, with values indicating means and error bars representing standard deviation.

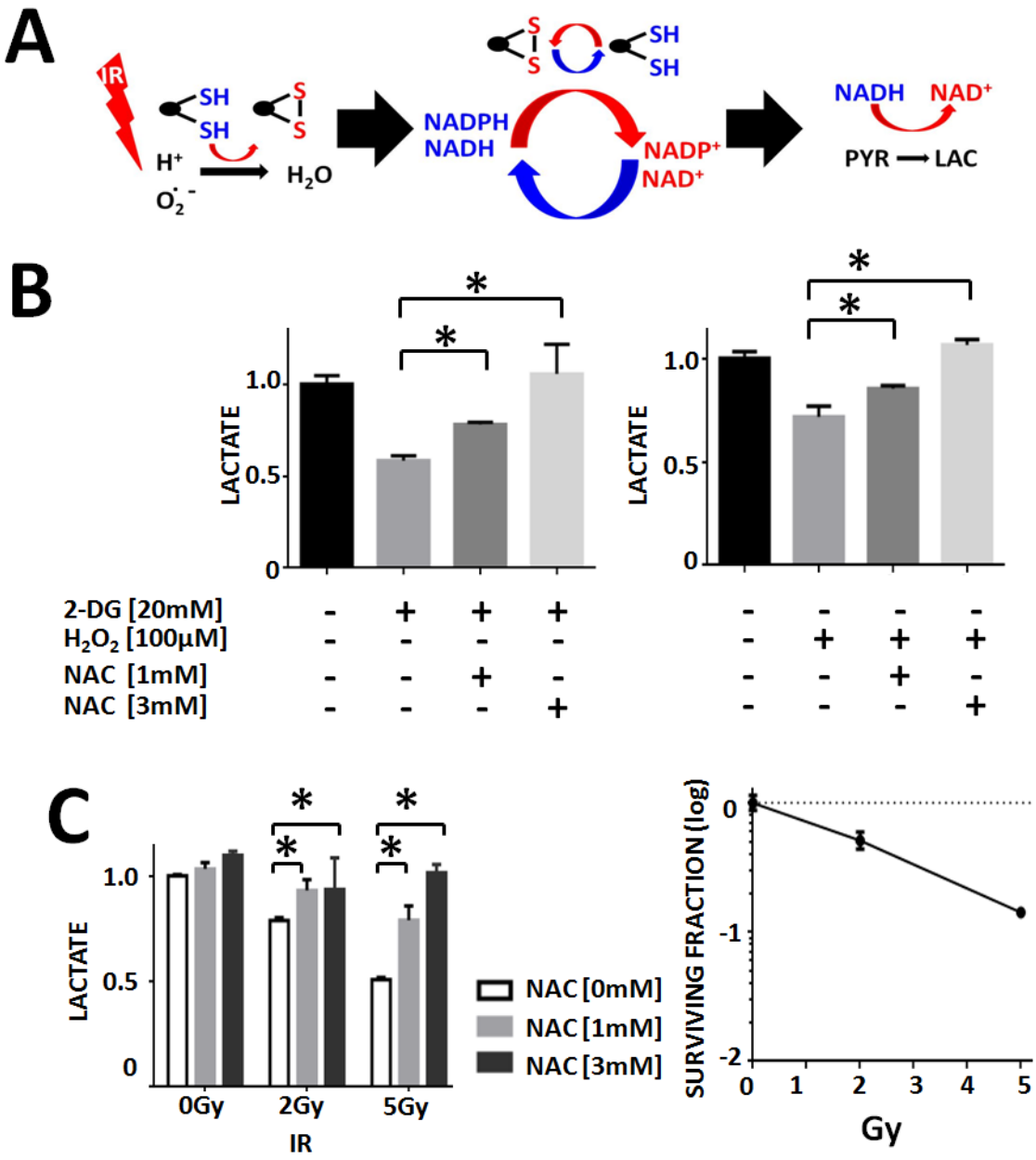

Figure 2. IR triggers a temporary, reversible perturbation in the cellular lactate production

A) Model of the hypothesized effects of IR on lactate production. B) Effects of metabolic inhibition or exogenous ROS on cellular lactate production. C) IR effects on lactate production correlated with relative cytotoxicity as measured using clonogenic survival following irradiation. These effects on lactate levels were reversed by treatment with NAC in a concentration-dependent manner. * indicates p-value < 0.05 compared to corresponding control condition. All values normalized to corresponding control condition (1.0). Each experiment was carried out at least in triplicate, with values indicating means and error bars representing standard deviation.

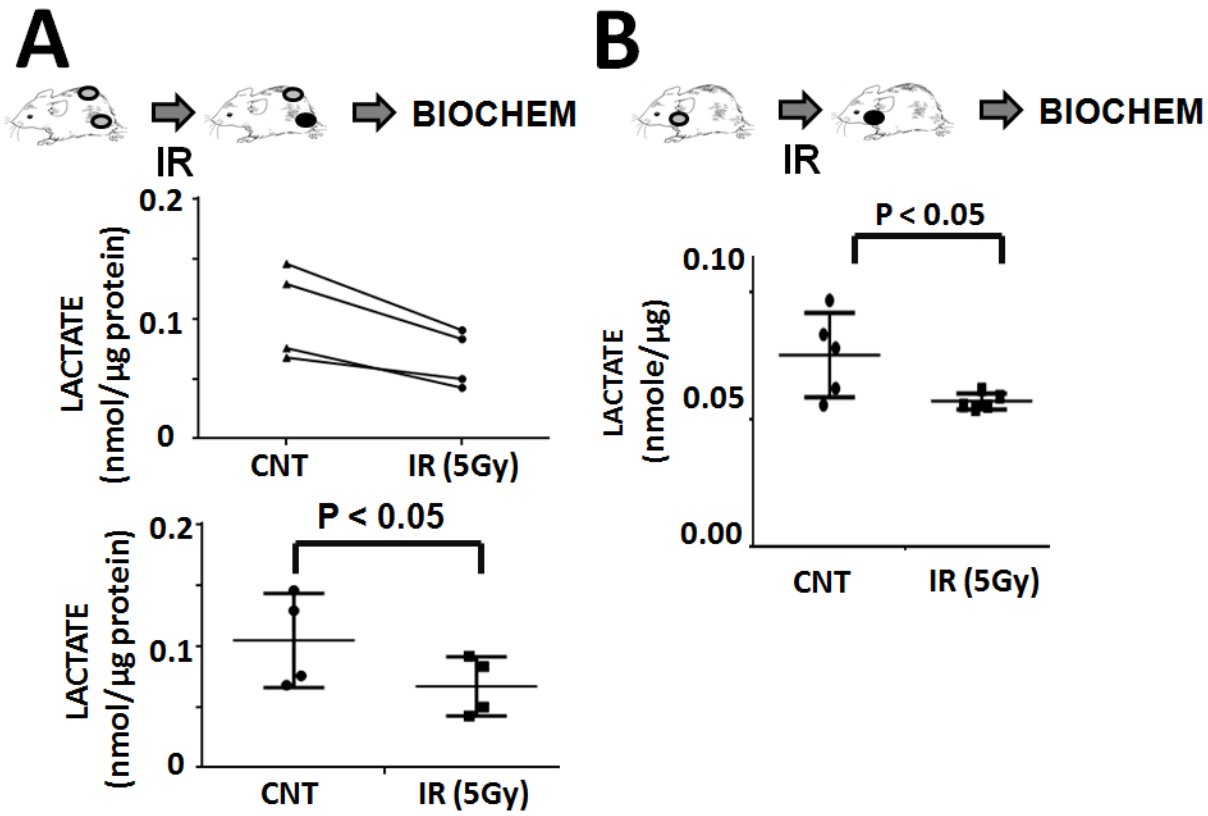

Figure 3. IR exposure acutely decreases tumor lactate levels

A) Bilateral flank tumors were created simultaneously. Tumors were allowed to grow. One set of tumors (n=4) was maintained as a control and the other set of tumors (n=4) irradiated to a total dose of 5 Gy. Immediately following irradiation, tumors were harvested. Tissue levels of lactate were measured and normalized to total protein content. Top panel illustrates paired tumor data, while bottom panel illustrates average data from control and irradiated tumor groups. **B)** Control (n=5) and irradiated (n=5; 5 Gy) orthotopic xenograft tumors were harvested immediately post-irradiation. Tissue levels of lactate were measured and normalized to total protein levels.

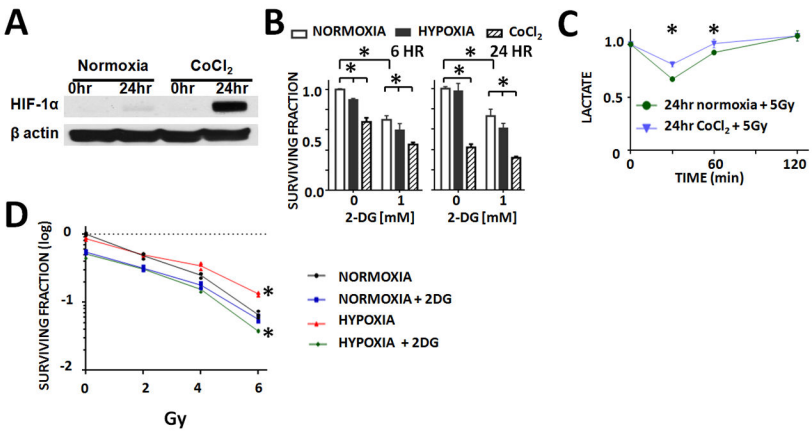

Figure 4. IR effects on lactate production persist in the presence of hypoxia and correspond to relative radiosensitivity/resistance

A) $CoCl_2$ exposure mimics hypoxia chamber exposure as demonstrated by HIF-1α induction. B) Hypoxia (chamber, 1% O_2) and $CoCl_2$ exposure increase sensitivity to 2-DG in a clonogenic survival assay. C) IR exposure triggers a transient, reversible drop in cellular lactate levels. This effect is diminished by approximately 50% following exposure to $CoCl_2$ for 24hr post-irradiation. All values normalized to corresponding control condition (1.0). D) Cells were exposed to increasing IR doses and effects of cell death ascertained using a clonogenic survival assay. 2-DG exposure radiosensitized tumors, while hypoxia (chamber, 1% O2) resulted in increased relative radioresistance. * indicates p-value < 0.05 compared to corresponding control condition. Each experiment was carried out at least in triplicate, with values indicating means and error bars representing standard deviation.

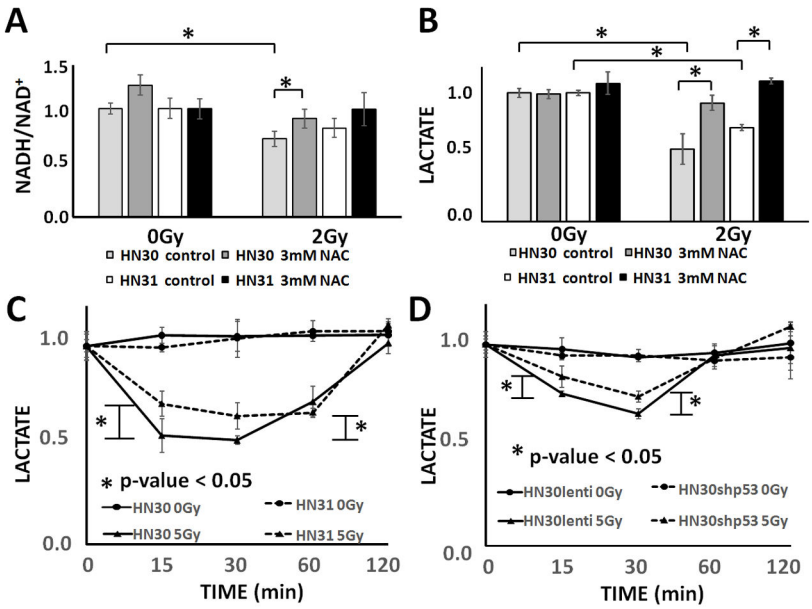

Figure 5. Acute IR effects on reducing potential and lactate can be used to detect intrinsic radioresistance driven by loss of p53 activity

A) HN30 (p53 wt) and HN31 (p53 mut) cells were exposed to IR (2 Gy) resulting in a transient, dose dependent, reversible (NAC) decrease in the NADH/NAD+ ratio. IR induced a proportionally larger decrease in cellular lactate levels in HN30 cells compared to their HN31 counterparts. B) HN30 and HN31 cells were exposed to IR (2 Gy) resulting in a transient, dose dependent, reversible (NAC) decrease in lactate levels. IR induced a proportionally larger decrease in cellular lactate levels in HN30 cells compared to their HN31 counterparts. C) IR (5 Gy) induced decreases in cellular lactate levels were blunted in HN31 cells compared to HN30 cells. D) IR induced decreases in cellular lactate levels were blunted in cells in which p53 activity was abrogated using shRNA (HN30shp53) compared to lentivirus transfected controls (HN30lenti). * indicates p-value < 0.05 compared to corresponding control condition. Each experiment was carried out at least in triplicate, with values indicating means and error bars representing standard deviation.

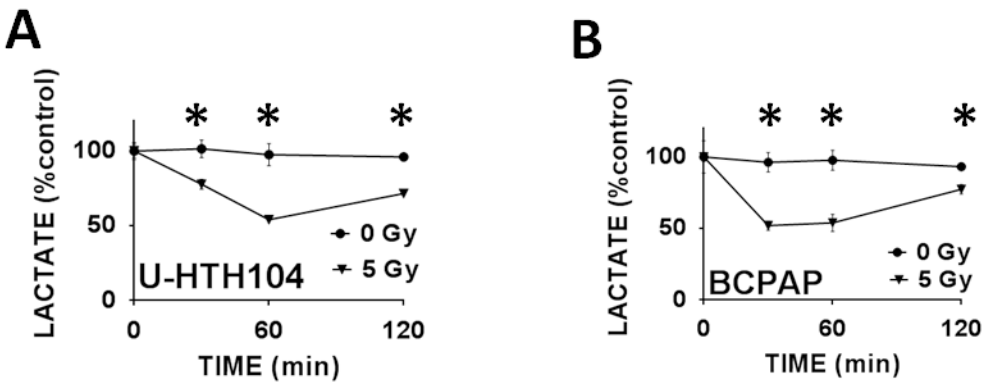

Figure 6. IR driven effects on cellular lactate levels are generalizable across multiple cell lines and histologies

ATC (A) and PTC (B) cells were exposed to IR. Lactate levels were measured as described above. * indicates p-value < 0.05 compared to corresponding control condition. Each experiment was carried out at least in triplicate, with values indicating means and error bars representing standard deviation.